Surface-structure dependence of water-related adsorbates on platinum

Badan, C.

Chapter 3

Experimental Set-up

3.1 Set-up

The experiments in this thesis were carried out using a custom-built vacuum (UHV) surface science chamber, called SHRIMP[1–3] (no acronym). It has a base pressure of 5x10 $^{-11}$ mbar and is equipped with two quadrupole mass spectrometers (QMS). One QMS (Baltzers, Prisma 200) protrudes into the main chamber and is mainly used for residual gas analysis (RGA). Figure 3.1 shows typical residual gases (hydrogen, water, CO, and CO_2) in our set-up after a bakeout. The other QMS (Balzers QMA 400) is kept in a differentially pumped canister that connects to the main UHV chamber via a circular spot with a radius of 2.5 mm, figure 3.2. It is positioned 2 mm from the face of the samples (Surface Preparation Laboratory, Zaandam, the Netherlands) during TPD studies.

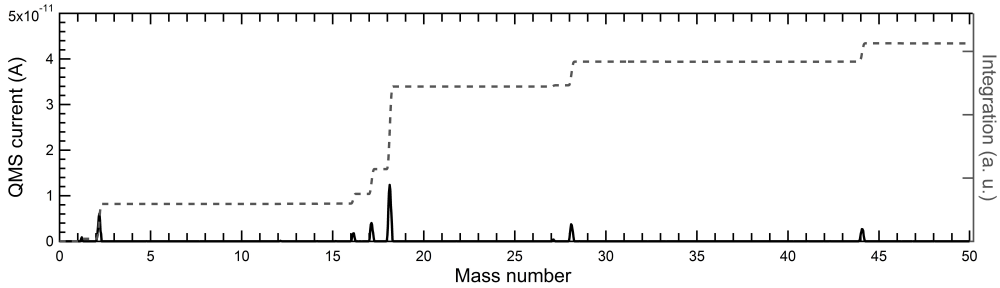

Figure 3.1: A typical residual gas analysis (RGA) after a bakeout shows the corresponding masses for H_2, H_2O, CO, and CO_2.

SHRIMP also contains a sputter gun (Prevac IS40C-PS) and LEED optics (VG

RVL 900). It has three directional dosers, which provide localized effusive dosing onto the sample. Our flat samples are 1 or 2 mm thick with 10 mm diameter, with a purity better than 5N and a an orientation alignment better than 0.1°. The sample can be cooled to 88 K using liquid N_2. Heating can be done radiatively by a filament (Osram, 150 W) mounted behind the sample. Samples can be also heated by electron bombardment using a positive voltage on the crystal assembly while the filament is grounded. For the crystals, temperature is measured with a type-K thermocouple laser welded to the top edge of the samples. For the temperature control, we use a PID controller (Eurotherm 2416) from which the thermocouple is electrically decoupled.

For TPD experiments the heating rate is 0.9 K s^{-1} over a temperature range of 250 K. H_2O from a Millipore Milli-Q gradient A10 system (18.2 MΩ cm resistance) was kept in a glass container and cleaned using multiple freeze-pump-thaw cycles. Before each set of experiments, these cycles were repeated to make sure that water has no contaminants. The glass container was exposed to 5.0 bar He (Linde gas, 5.0). For water and O_2 TPD, the adsorption temperature is below 100 K. To avoid adsorbing H_2 or other residual gases on the surfaces, D_2 is dosed while cooling the sample, between 700 - 100 K. A blank TPD experiment did not yield any H_2, D_2, H_2O or O_2 desorption. To provide minimum contamination on the surface, we turned off all filaments while dosing.

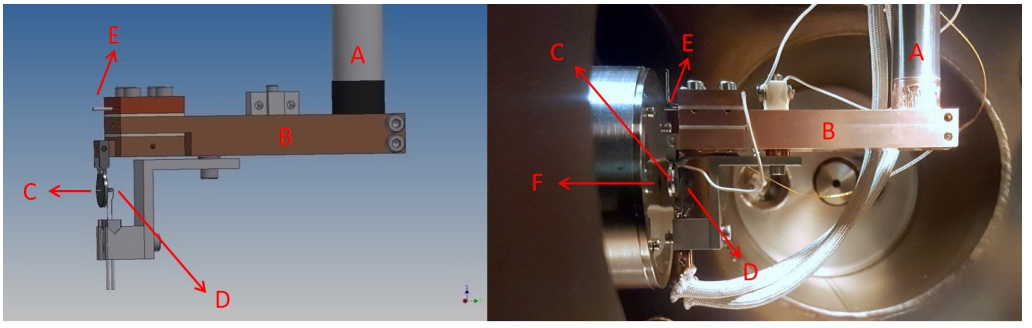

Figure 3.2: TPD studies are performed with a differentially pumped QMS. For the experiments, the samples are positioned 2 mm from the QMS. In our setup, a cryostat manipulator (A) is connected to a copper sample-holder (B). A 150 W filament (D) is attached behind the sample (C). The distance of the sample to the QMS canister (F) is reproduced using a pin (E).

3.2 Temperature programmed desorption

For an accurate kinetic analysis (see chapter 2), a proper background subtraction is needed. Especially when water is dosed onto a sample, we find that stainless steel will also adsorb water. The high vacuum time constant of water results in an increase in the baseline of the water TPD spectra. To remove this effect, we use the following approximation, equation 3.1, to define the baseline (y).

$$\mathrm{y}=\mathrm{y}_0+\frac{1}{2}\triangle\mathrm{y}\times\left(\tanh\left(\frac{T-T_0}{\triangle T}\right)+1\right) \tag{3.1}$$

$\triangle$y = total increase in the height of baseline

T_0 = center of the S-curve (an s-shaped function with finite limits at negative and positive infinities) before T_M

$\triangle$T = arbitrary parameter to smooth out the tanh

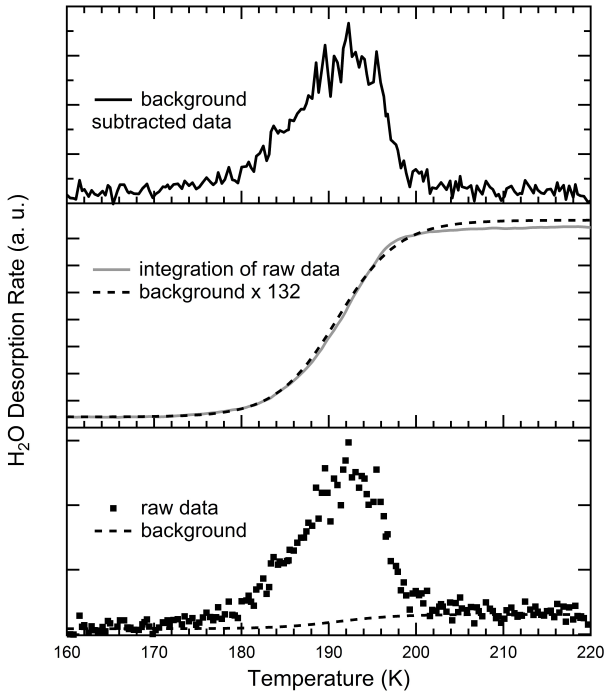

Figure 3.3: Because water sticks to the stainless steel walls of the chamber, the vacuum time constant of H_2O yields an increase in the background of water TPD spectra. An accurate approximation to subtract this baseline is given in equation 3.1. The bottom panel shows a TPD spectrum of water from Pt(211). The middle panel compares the approximation derived by using equation 3.1 with the integrated TPD spectrum. The top panel show the background subtracted spectrum.

Figure 3.3 exemplifies the background subtraction process for a TPD spectrum[4, 5]. In the bottom panel, we obtain a baseline using the approximation described above (equation 3.1). In the middle panel, we compare the baseline curve with the integrated TPD spectrum. As the integral reflects the development of the TPD curve at any point in time, it is crucial that the shape of the baseline curve develops similarly to the TPD spectrum. The top panel shows the baseline subtracted TPD spectrum. We verified that this method does not influence the baseline of the leading edges. In this thesis, all spectra are baseline corrected.

3.3 Low energy electron diffraction

Low electron energy diffraction (LEED) is a very common technique used to determine the surface structure. It uses a well-defined normal incidence of the primary electron beam on the sample. The electrons are scattered back elastically from the well-ordered surface crystallography in all directions. Diffracted electrons are selected by energy filtering grids, before landing on the phosphorescent screen. The well-ordered structure of the surface creates a direct image of the reciprocal lattice of the surface[6, 7].

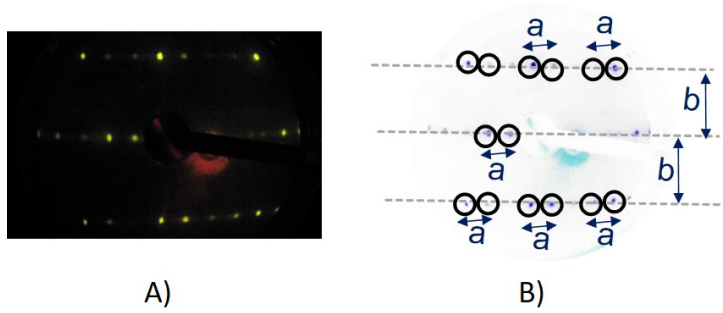

Figure 3.4: Raw (A) and color-inverted (B) LEED images of a clean Pt(221). The average ratio of spot row spacing b over spot splitting a yields 3.06. This agrees well with literature value of 3.00[8].

The surface structure type can be determined by row spacing to spot splitting ratio[8]. In figure 3.4, we show an exemplary picture of a LEED pattern created by a clean Pt(221) surface. From this image we extract a row spacing over spot splitting ratio of 3.06, which is in good agreement with the tabulated value of 3.00[8]. This agreement indicates long-range order with the expected average terrace width. We repeated the same analysis for other samples (Pt(111), Pt(211), Pt(221), Pt(533) and Pt(553)) used in this research and also found excellent agreements with literature values.

In addition to average terrace width, the step height can also be determined with LEED. This analysis is done by assigning the electron energies (E_{el}) at which the (00) beam shows singlets and doublets[9]. Henzler[10] derived a means to determine the step height as a function of energy as shown in equation 3.2.

$$V_{00} = \frac{150}{4} \times \frac{s^2}{d^2} \tag{3.2}$$

where V_{00} is the energy of the incoming electrons in eV, d is the step height in Å and s is an (unknown) integer for singlet spot appearance and half integer for doublet spot appearance.

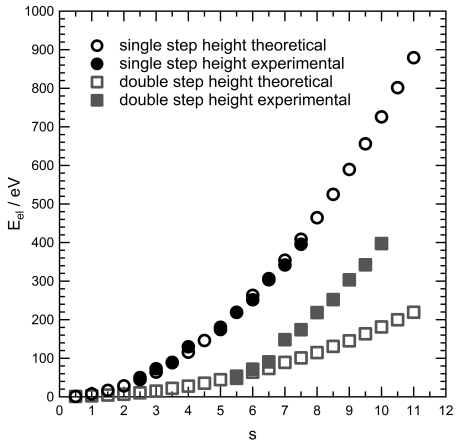

Figure 3.5: The step height analysis of Pt(533) using equation 3.2. Open circles: theoretical values of E_{el} for s with one-atom high steps. Open squares: theoretical values of E_{el} for s with two-atom high steps. Closed circles and squares are the fit of experimental data for s with one and two atomic high steps, respectively[11].

Figure 3.5 compares the theoretical and experimental energies of different s for single and double step heights on Pt(533), equation 3.2. The open circles and open squares are theoretical energies at various values of s for both one and two atom high steps, respectively. The closed circles and closed squares shows the obtained experimental E_{el} for single and double step heights[11]. The figure clearly shows that the circles coincide accurately whereas the squares do not. This analysis proves that Pt(533) consists of steps separated by single atoms. Applying the same (00) analysis on different spots of the sample confirms that the anticipated structure is well-defined over the entire crystal. With the same method, we confirmed that all the high-miller-index samples used in this thesis have monoatomic step height.

3.4 Bibliography

References

(1) Badan, C.; Koper, M. T. M.; Juurlink, L. B. F. *The Journal of Physical Chemistry C* **2015**, *119*, 13551–13560.

(2) Badan, C.; Heyrich, Y.; Koper, M. T. M.; Juurlink, L. B. F. *The Journal of Physical Chemistry Letters* **2016**, 1682–1685.

(3) Badan, C.; Farber, R. G.; Heyrich, Y.; Koper, M. T.; Killelea, D. R.; Juurlink, L. B. *The Journal of Physical Chemistry C* **2016**, *120*, 22927–22935.

(4) Van der Niet, M. J. T. C.; den Dunnen, A.; Juurlink, L. B. F.; Koper, M. T. M. *Journal of Chemical Physics* **2010**, *132*, 174705–174713.

(5) Van der Niet, M. J. T. C.; den Dunnen, A.; Juurlink, L. B. F.; Koper, M. T. M. *Physical Chemistry Chemical Physics* **2011**, *13*, 1629–1638.

(6) Ellis, W. P. *Surface Science* **1974**, *45*, 569–584.

(7) Ellis, W. P.; Schwoebel, R. L. *Surface Science* **1968**, *11*, 82–98.

(8) Vanhove, M. A.; Somorjai, G. A. *Surface Science* **1980**, *92*, 489–518.

(9) Mom, R. V.; Hahn, C.; Jacobse, L.; Juurlink, L. B. *Surface Science* **2013**, *613*, 15–20.

(10) Henzler, M *Surface Science* **1970**, *19*, 159–171.

(11) Van der Ham, K. Working Towards Ethanol Dissociation on Pt(533)., MA thesis, the Netherlands: Leiden Institute of Chemistry, Leiden University, 2013.